A novel heteroleptic Cu(II)-phenanthroline-UDCA complex as lipoxygenase inhibitor and ER-stress inducer in cancer cell lines

Sebastiano Masuri [a], Lukáš Moráň [b,c], Tereza Vesselá [b], Enzo Cadoni [a], Maria Grazia Cabiddu [a], Lukáš Pečinka [d], Viktorie Gabrielová [b], Francesca Meloni [a], Josef Havel [d,e], Petr Vaňhara [b,d], Tiziana Pivetta [a,*]

[a] *Department of Chemical and Geological Sciences, University of Cagliari, Cittadella Universitaria, 09042, Monserrato, Cagliari, Italy*
[b] *Department of Histology and Embryology, Faculty of Medicine, Masaryk University, 62500 Brno, Czech Republic*
[c] *Research Centre for Applied Molecular Oncology, Masaryk Memorial Cancer Institute, 65653 Brno, Czech Republic*
[d] *Department of Chemistry, Faculty of Science, Masaryk University, 62500 Brno, Czech Republic*
[e] *International Clinical Research Center, St. Anne's University Hospital, 65691 Brno, Czech Republic*

ARTICLE INFO

ABSTRACT

A new heteroleptic copper(II) compound named C0-UDCA was prepared by reaction of $[Cu(phen)_2(OH_2)](ClO_4)_2$ (C0) with the bile ursodeoxycholic acid (UDCA). The resulting compound is able to inhibit the lipoxygenase enzyme showing more efficacy than the precursors C0 and UDCA. Molecular docking simulations clarified the interactions with the enzyme as due to allosteric modulation. The new complex shows antitumoral effect on ovarian (SKOV-3) and pancreatic (PANC-1) cancer cells at the Endoplasmic Reticulum (ER) level by activating the Unfolded Protein Response. In particular, the chaperone BiP, the pro-apoptotic protein CHOP and the transcription factor ATF6 are upregulated in the presence of C0-UDCA. The combination of Intact Cell MALDI-MS and statistical analysis have allowed us to discriminate between untreated and treated cells based on their mass spectrometry fingerprints.

1. Introduction

Bile acids are hydroxylated steroid acids biosynthesized from cholesterol and predominantly found in the bile of mammals and other vertebrates. They are classified as primary (i.e., cholic acid CA, cheno-deoxycolic acid CDA), whose biosynthesis take place in liver cells, and secondary (i.e., deoxycholic acid DCA, ursodeoxycholic acid UDCA), that are obtained from the primary ones through biochemical processes performed by intestinal bacteria [1]. Bile acids are involved in cholesterol catabolism and emulsification of lipid in the intestinal tract. In addition these compounds work as endocrine mediators activating several receptors (e.g. nuclear farnesoid X receptor (FXR) and pregnane X receptor (PXR), the G-protein coupled receptor TGR5, etc) that are involved in pathways such as glucose and lipid metabolisms [2]. UDCA (Fig. 1A) is currently approved for the treatment of primary biliary cirrhosis and other cholestatic disorders [3,4] In addition, this

compound has shown to possess modulable activity, cytoprotective or cytotoxic, according to the treated cell-type [5]. Studies of UDCA in combination with conventional anticancer drugs have pointed out that UDCA is able to attenuate some of their common side effects [6]. After the discovery of cisplatin's cytotoxic properties, several metal complexes were prepared and tested for their biological activity, exploiting different action mechanisms such as redox reaction, photo and thermal activation, catalytic pathways, and many others [7]. Also copper-based metallodrugs have been prepared and tested with the aim of designing novel anticancer compounds having an optimal toxicological profile [8–12]. The biological activity of these copper complexes is exerted by mechanisms that might involve different targets or different reactions. The most common target appears to be the DNA [13], but some copper complexes were identified as tumour specific proteasome inhibitors [14]. Also the redox reactions [15] are involved, depending on the redox potential of the complexes, that in turn depends on the coordinating

ligands that can stabilize the oxidation state II of the metal ion, or promote the reduction by a geometry template effect, mediated by the solvent [16].

Previous studies carried out in our research group have shown that Cu(II) complexes such as [Cu(phen)$_2$(OH$_2$)](ClO$_4$)$_2$ (C0, Fig. 1B), [Cu(phen)$_2$(L)](ClO$_4$)$_2$ (where L are imidazolidine-2-thione and some *N*-alkylated derivatives) and [Cu(phen)$_2$(Salubrinal)](ClO$_4$)$_2$ are able to induce massive cell death in ovarian cancer cells (A-2780, SKOV-3) by activating the pro-apoptotic branch of the Unfolded Protein Response (UPR) [17,18]. UPR is a coordinating adaptive program that responds to accumulation of improperly folded proteins in the endoplasmic reticulum (ER), a condition known as ER stress. Initiation of UPR can lead to adaptation or apoptosis, especially in a condition of prolonged or severe ER stress [19]. This pathway has been targeted by other anticancer copper complexes as well. For instance, the Cu(I)-phosphine complex of Gandin and coworkers shows high anticancer potency on different leukemia and colon cancer cells and interferes at the ER level by causing an overexpression of different UPR-related markers [20,21]. The Cu(II) triazole-based complex developed by Tardito et al., showed ER-related alterations at morphological and molecular level on a panel of different cancer cells [22]. Notably, Balsa and colleagues have pointed out the induction of UPR in triple negative breast cancers treated with their Cu(II) hydrazone-based complexes [23].

Moreover, UDCA and its taurine-conjugated derivative (taursodeoxycholic acid, TUDCA), have been extensively studied as ER stress modulators, and proved to exert their cytoprotective activity acting as chemical chaperones [24,25]. Previous studies of TUDCA in combination with the mixed Cu(II) phenanthroline complexes earlier cited, have shown how the cytotoxicity of these compounds might be modulated by the presence of TUDCA itself [17,18].

Given these premises and considering that UDCA comprises a carboxylic group that might interact with Cu(II), we prepared a new heteroleptic copper complex from C0 and UDCA, named C0-UDCA, aiming to exploit the biochemical activities of the two precursors (Fig. 1C).

The coordination mode, the solution equilibria, the antioxidant and anti-lipoxygenase activity of this novel compound were assessed by means of different experimental and theoretical studies. The cytotoxic activity of C0-UDCA against ovarian (SKOV-3) and pancreatic (PANC1) cancer cells was evaluated in-vitro and compared to results obtained for its synthetic, previously characterized, precursor C0. Moreover, based on previous studies where we showed the potentialities of intact cell mass spectrometry as a tool for cell quality control, bio-typing, and rapid identification of cell phenotype changes [26,27], we verified whether we would be able to discriminate differential cell responses to the investigated compounds.
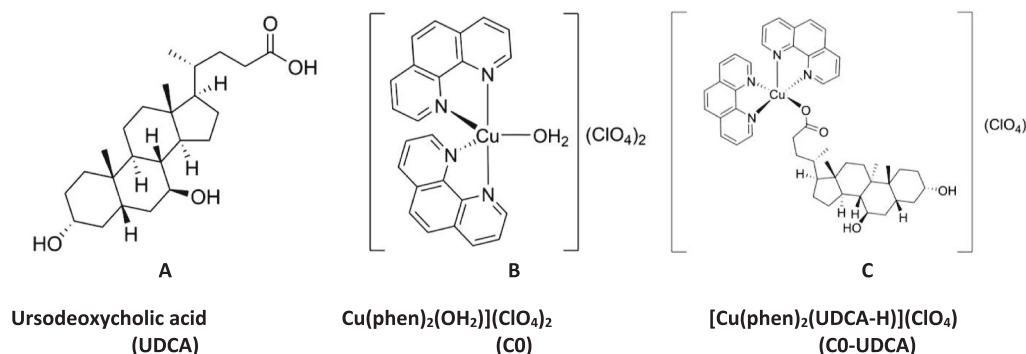
2. Results and discussion

2.1. Synthesis and characterization of C0-UDCA

The reaction between the blue-green C0 and the colourless sodium salt of UDCA (NaC$_{24}$H$_{39}$O$_4$) led to the green complex [Cu(phen)$_2$(C$_{24}$H$_{39}$O$_4$)](ClO$_4$) (C0-UDCA), whose stoichiometry has been established by elemental analysis (see experimental part) and mass spectrometry. In the ESI-MS spectrum of C0-UDCA (Fig. 2) a peak at 814 *m/z* was observed, corresponding to the [Cu(phen)$_2$(UDCA-H)]$^+$ ion, obtained from the ionization of the neutral [Cu(phen)$_2$(UDCA-H)](ClO$_4$) species. Other peaks, at 634, 457, 243 and 181 *m/z* corresponded to fragments of the molecular ion, observed depending on the experimental conditions. Precursor ion scan experiments showed that the fragments were originated in ESI-phase by the precursor [Cu(phen)$_2$(UDCA-H)]$^+$: i) the peak at 634 *m/z* was originated by loss of a phenanthroline unit to give the species [Cu(phen)(UDCA-H)]$^+$; ii) the peak at 243 *m/z* was originated by loss of one phenanthroline unit and the UDCA ligand, with the reduction of the metal ion, to give the species [Cu(phen)]$^+$ (the reduction of Cu(II) to Cu(I) is widely observed in ESI phase, depending on the used solvent) [28]; iii) finally, the peak at 181 *m/z* was due to the protonated phenanthroline species [phen+H]$^+$. The identity of the reported ions was confirmed by the fitting of the isotopic patterns (Fig. S1) and tandem mass experiments (see Mass spectrometry). High-resolution mass spectrum of C0-UDCA in the range 600–850 *m/z* was recorded to further confirm the composition of the peaks at 814 *m/z* and of its
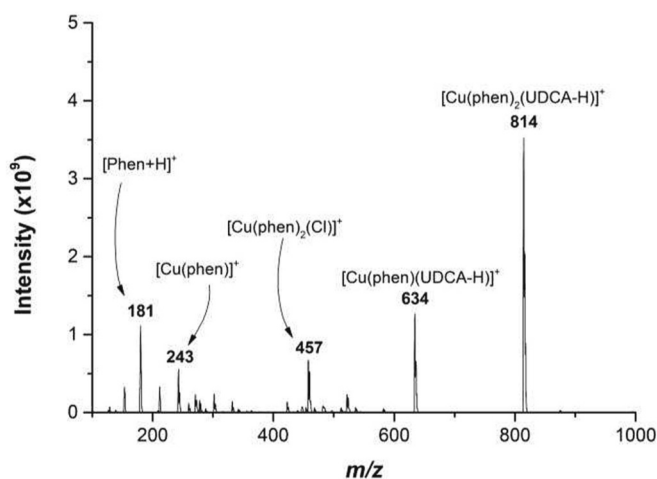
Fig. 2. ESI-MS spectrum of [Cu(phen)$_2$(UDCA-H)](ClO$_4$) (methanol:water 1:1, 5000 V at capillary). All the mass values are expressed as monoisotopic masses, computed as the sum of the masses of the primary isotope of each atom in the molecule (note that the monoisotopic mass may differ from the nominal molecular mass, especially for big molecules).

Fig. 1. Molecular structures and acronyms of the studied compounds.

fragment at 634 *m/z* (Fig. 3A). As observable, the fitting of the isotopic pattern (Fig. 3B) and the matching between experimental and calculated exact masses (814.3532 u vs 814.3519 u and 634.2844 u vs 634.2832 u) confirmed the proposed stoichiometry.

The novel copper complex [Cu(phen)$_2$(UDCA-H)](ClO$_4$) proved to be stable in the solid state at room temperature, without precautions. It is not deliquescent. As regards its solubility, C0-UDCA is soluble in DMSO at 0.1 M concentration level, in CH$_3$CN at 0.01 M, in the H$_2$O:CH$_3$CN mixture (1:1) at 8 mM and in CH$_3$OH:H$_2$O at micromolar concentration. Solubility in water could be enhanced (up to 0.5 mM) by dissolving C0-UDCA in a minimal amount of DMSO at 40 °C prior to water addition. In this case, sonication or vigorous mixing should be avoided to prevent the formation of emulsions. Stock solutions of C0-UDCA in DMSO or CH$_3$CN are stable at 4 °C up to 6 months, while stock solutions in H$_2$O:CH$_3$CN mixture (1:1) could be stored at 25 °C for 2 weeks. The stability of C0-UDCA in phosphate buffer was assessed by following the spectral variation in the 200–325 nm range for 24 h recording 1 spectrum every 60 min (Fig. S2). No significant variations in the shape and intensity of the spectra were observed.

2.2. Complex formation constant of C0-UDCA

The complex formation constant was studied in 0.05 M phosphate buffer at pH 7.4. At this pH UDCA is present as monoanionic species due to the proton loss from the carboxylic moiety. The method of continuous variation (Job's method) was applied to determine the number of the formed complexes and the related stoichiometry. [29,30] Absorption spectra collected varying the reactants molar fractions are reported in Fig. S3A, while the absorbance at 271 nm, corrected for the absorption of pure species, is reported as a function of the ligand molar fraction in Fig. S3B. These data clearly show the formation of a 1:1 ligand to metal complex ($\chi_L = 0.49$).

Once established the formation of a unique 1:1 ligand to metal complex, the related formation constant was determined by spectrophotometric titrations. Selected spectra recorded during the titration of C0 with deprotonated UDCA are reported in Fig. 4, corrected for the dilution. As observable, the addition of the ligand resulted in a slight increment of the absorbance at 271 nm, until the ligand/metal molar ratio reached the unity value (see inset in Fig. 4 (upper)). The Factor Analysis of the spectrophotometric data indicated three linearly
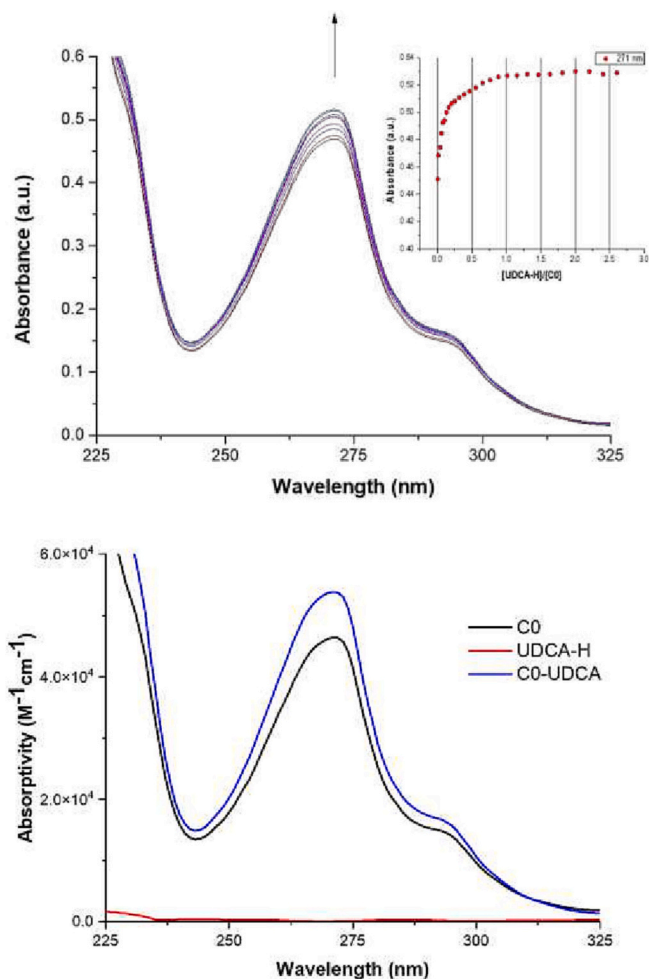

Fig. 4. Selected spectra collected during the titration of (upper) 2.12×10^{-5} mmol of C0 with UDCA-H (2.55×10^{-5} M) in 225–325 nm range, corrected for the dilution; (bottom) absorptivity spectra of C0, UDCA-H and C0-UDCA (phosphate buffer 0.05 M, pH 7.4, 25 °C, 1 cm optical path length).

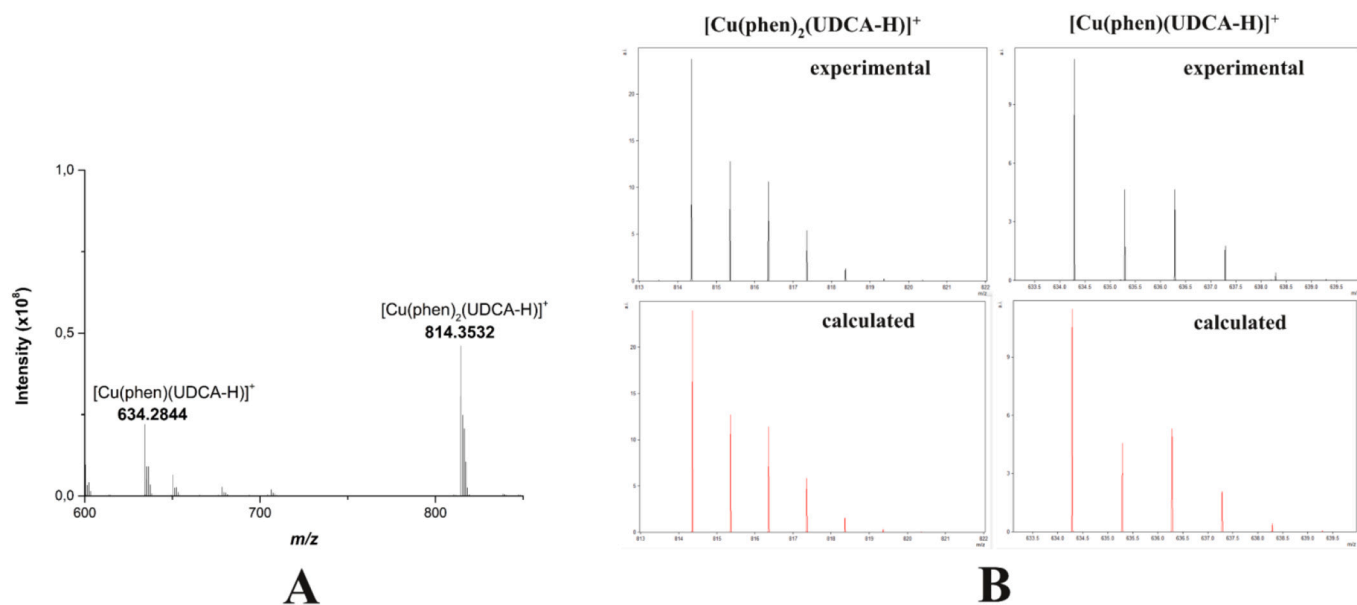

Fig. 3. (A) High-resolution mass spectrum of C0-UDCA in the 600–850 *m/z* range, (B) experimental and calculated isotopic pattern for peaks at 814 and 634 *m/z*, (methanol:water 1:1). All the mass values are expressed as monoisotopic masses.

independent absorbing species in solution, i.e., the two reactants and the formed complex. The complex formation constant, expressed as log β, was calculated as 5.2 ± 0.2 M^{-1}. The pure spectra of the reactants and the formed complex are reported in Fig. 4 (bottom). The absorption bands of C0 and C0-UDCA fall in the same region, however the mixed complex shows absorptivity value higher at 271 nm.

2.3. Coordination mode in C0-UDCA

Since any attempt to obtain single crystals suitable for X-ray analysis was unsuccessful, the coordination mode for the novel C0-UDCA complex was proposed by combining the experimental data (UV–Vis, IR spectroscopy, ESI-MS and tandem MS spectrometry) with the theoretical calculations.

2.3.1. UV–Vis

The absorption spectrum of C0-UDCA in CH$_3$CN:H$_2$O (1:1) solution in the region 450–1100 nm is reported in Fig. S4 and features a maximum at 686 nm and a shoulder at 942 nm. In analogy with the absorption spectra of variously ternary Cu(II) bis-phenanthroline complexes previously characterized, [31] a penta-coordinated geometry might be proposed also for the novel complex C0-UDCA.

2.3.2. FT-IR

FT-IR spectrum of C0-UDCA (Fig. S5C) shows a large and intense band at 3410 cm^{-1}, that can be ascribed to the hydroxyl groups of the UDCA moiety, while the two peaks at 2933 and 2865 cm^{-1} are relative to the -CH- stretching frequencies. Asymmetric and symmetric stretching peaks of oxygen carboxylate group ($v_{asym}(OCO)$ and $v_{sym}(OCO)$) fall at 1565 and 1375 cm^{-1} respectively. In the FT-IR spectrum of sodium ursodeoxycholate (Fig. S5A) the same bands appear at 1561 and 1406 cm^{-1} respectively. The parameter $\Delta(OCO) = v_{asym}(OCO) - v_{sym}(OCO)$ is commonly used to gain more insights regarding the coordination mode of carboxylate functional groups in metal complexes. In particular, a $\Delta(OCO)complex > \Delta(OCO)ligand$ is indicative of an unidentate coordination mode of the carboxylic group. [31,32] Considering that $\Delta(OCO)$ for C0-UDCA equals to 190 cm^{-1}, which is higher than the same value for sodium ursodeoxycholate (155 cm^{-1}), we can assume that also for C0-UDCA coordination of carboxylate group to the metal centre takes place in mono-dentate fashion. Signals of the phen moieties are visible at 3068, 1519, 1430, 1386, 851, 724, 624 cm^{-1} (see for comparison IR spectrum of the precursor C0, Fig. S5B), while the wide band in the region 1150–1030 is due to the perchlorate anion.

2.3.3. Mass spectrometry

Tandem MS experiments at different collision energies (CE) were performed to identify the nature of the peaks containing Copper (II), phenanthroline and UDCA and give more insights about the structure of the novel C0-UDCA complex. As regards the ion [Cu(phen)$_2$(UDCA-H)]$^+$ (m/z 814), the formation of a product ion at m/z 634 is evidenced from 5 V (Fig. 5). The former ion, whose formula was previously proposed as [Cu(phen)(UDCA-H)]$^+$, is originated from precursor at m/z 814 by loss of one phenanthroline unit (Fig. S6A). As observed in Fig. 5, a gradual decrease in intensity for the peak at m/z 634 is observed, as CE is further increased (from 30 V). This feature is consistent with further fragmentation processes of the former ion. In particular, from 35 V, two peaks at m/z 260, [Cu(phen)(OH)]$^+$, and 243, [Cu(phen)]$^+$, were observed. The first product ion might come from its precursor by the rearrangement showed in Fig. S6B, i.e., transposition of a Hα from UDCA moiety and subsequent closure of a Cα = Ccarbonyl double bond with loss of a neutral ketene. The second fragment is originated by the radical process depicted in Fig. S6C, which brings to a Cu(I) ion with the loss of the UDCA moiety as a radical. Collision induced fragmentation experiments performed on the ion at m/z 634 (Fig. S7) showed the same pattern, thus confirming the fragmentation scheme previously reported. The
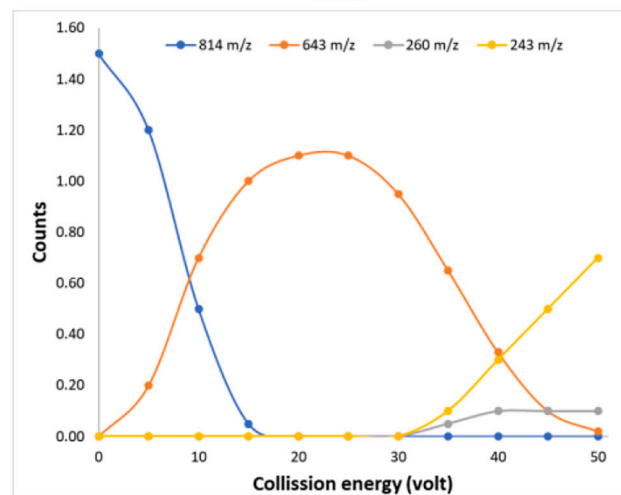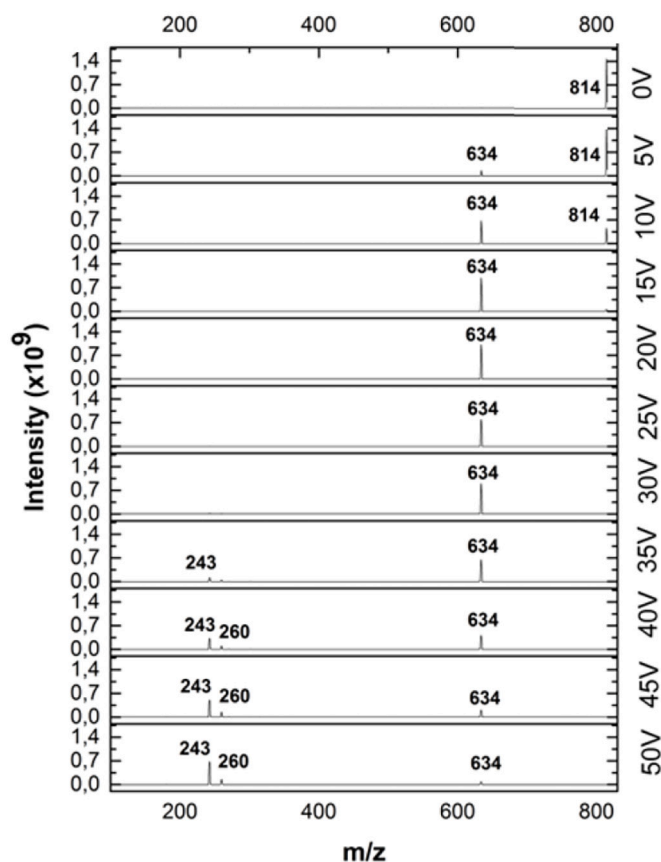

Fig. 5. Tandem MS fragmentations and breakdown curves at different collision energy (0–50 V).

breakdown curves, obtained reporting the peak intensity vs CE, show the relative stability of the formed species: i) at 0 CE the unique stable species is [Cu(phen)$_2$(UDCA-H)]$^+$; ii) it is necessary to apply 20 V as CE to completely convert [Cu(phen)$_2$(UDCA-H)]$^+$ in [Cu(phen)(UDCA-H)]$^+$; iii) at CE higher than 30 V [Cu(phen)(UDCA-H)]$^+$ is fragmented with loss of the UDCA ligand.

2.3.4. DFT calculations

Geometry optimization for both UDCA-H and Cu(II) complex [Cu(phen)$_2$(UDCA-H)]$^+$ were performed using the same computational setup employed for the parent copper complex [Cu(phen)$_2$(OH$_2$)]$^+$ and other similar Cu(II) complexes, as previously reported [18].

In particular, assessment of the DFT performance for [Cu

(phen)$_2$(OH$_2$)]$^+$ (whose coordinates were taken from C0 single X-Ray structural data) revealed a very good agreement between experimental and calculated data. In Fig. S8A DFT, optimized geometry for UDCA-H ligand is reported. As observable from frontier molecular orbital analysis (Fig. S8B), HOMO and HOMO-1 molecular orbitals are highly centred on oxygen carboxylate moiety, thus supporting a coordination from this functional group. Selected bonds, angles and dihedrals are reported in Table S1.

Geometry optimization at DFT level for [Cu(phen)$_2$(UDCA-H)]$^+$ reveals a geometry closer to a square pyramidal than to a trigonal bipyramidal, as suggested by the value of geometrical parameter $\tau = \frac{\beta-\alpha}{60°}$ of 0.22. [33] The former distortion is also evident at bond lengths level, where elongation of Cu—N2 (2.309 Å) is accompanied by shortening of Cu—N3, Cu—N1 and Cu—O1 bonds (2.040, 2.059 and 1.958 Å respectively). These results are in agreement with several mono and binuclear Cu(II) bis-phenanthroline complexes coordinated by carboxylate functional groups [34–37] (Table S2). Atomic charges, computed at NPA level (Table S3), show on copper ion a significant lower atomic charge (1.39) compared with its formal charge +2, while on N1–4 and O1 atoms high negative calculated charges were evidenced. This trend suggests a partial charge transfer to the metal centre from the coordinating atoms of ligands, as evidenced at frontier Molecular Orbital level, where both α and β SOMOs are centred on UDCA moiety, while α and β LUMOs are redistributed among the metal centre and one of the phenanthroline ligands (Fig. 6).

2.4. Soybean lipoxygenase inhibition: experimental study

Lipoxygenases constitute a widespread group of Iron dioxygenases that are involved in the production of leukotrienes through the arachidonic cascade pathway. [38] Increased levels of human lipoxygenases, such as 5-LOX, have been observed in several types of cancer, including pancreatic [39], bladder [40], oesophageal [41], hepatocellular [42], colon [43], and prostatic [44] cancer cells. Moreover, the inhibition of 5-LOX activity by several small molecules have proved to arrest the tumour cell proliferation and induce apoptosis [45]. For this reason, we studied the inhibition of the UDCA and C0-UDCA towards these enzymes using Soybean Lipoxygenase as the model. The experiments were performed keeping constant the concentration of substrate and enzyme and varying that of UDCA, or C0-UDCA. The results obtained were compared with the ones obtained for C0 [18]. In the absence of an inhibitor, the enzyme requires about 90 min to convert the linoleate substrate to 13-hydroperoxylinoleic. In the presence of UDCA, the substrate conversion is reduced till the 80% but it is required a concentration of 600 microM (Figs. 7A and S9A). In the presence of C0-UDCA, the inhibition appears more potent, being almost complete at approx. 9 microM (Figs. 7B and S9B).

The inhibition percentage (IP) varies with the time for every given concentration (Fig. S10), becoming invariant after 50 min for UDCA and 35 min for C0-UDCA. These two values were chosen as the time reference to calculate the IC$_{50}$ value, i.e., the concentration required to inhibit 50% of enzyme activity. For the two compounds, IC$_{50}$ resulted to be 69 ± 7 μM for UDCA and 4.4 ± 0.1 μM for C0-UDCA (Fig. 7B). Since
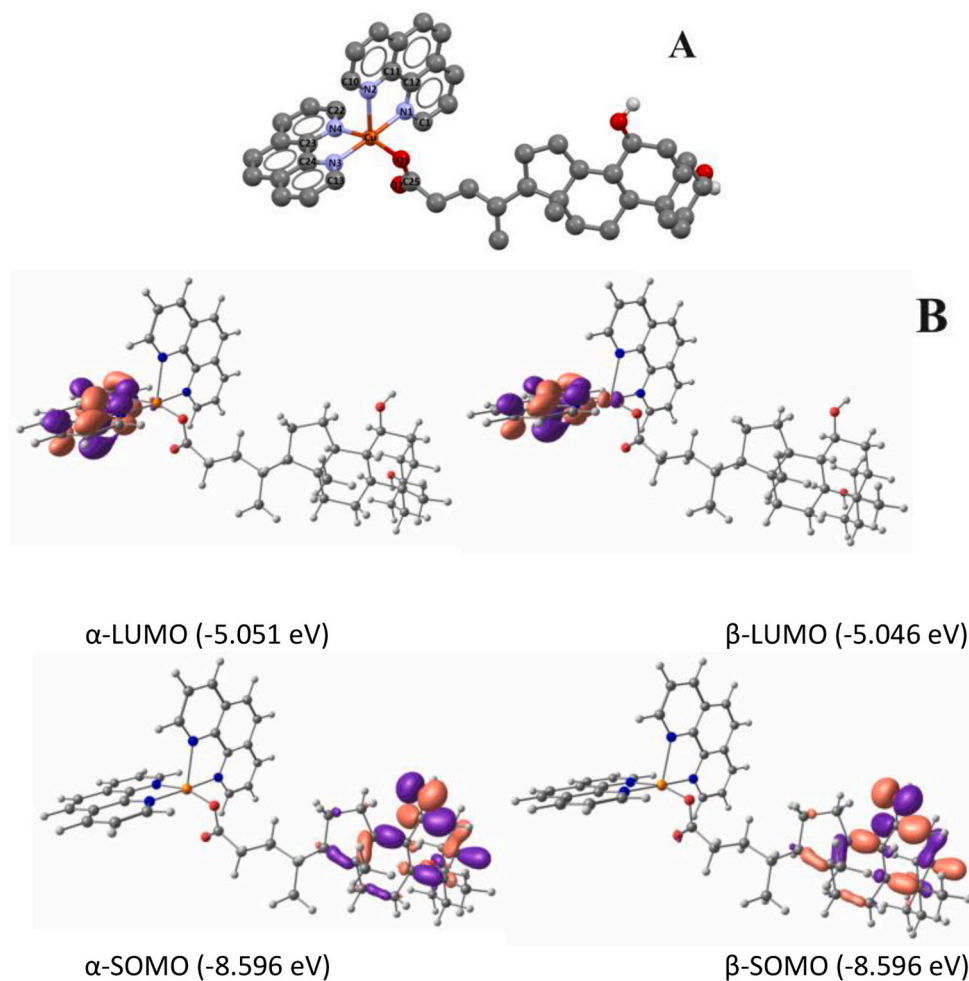

Fig. 6. Molecular drawings and atom labelling schemes for [Cu(phen)$_2$(UDCA-H)]$^+$ (A) at the DFT-optimized geometry. Isosurface drawings of selected frontier molecular orbitals calculated (B) for [Cu(phen)$_2$(UDCA-H)]$^+$ (contour value: 0.05). Non-polar hydrogen atoms in (A) are omitted for clarity.
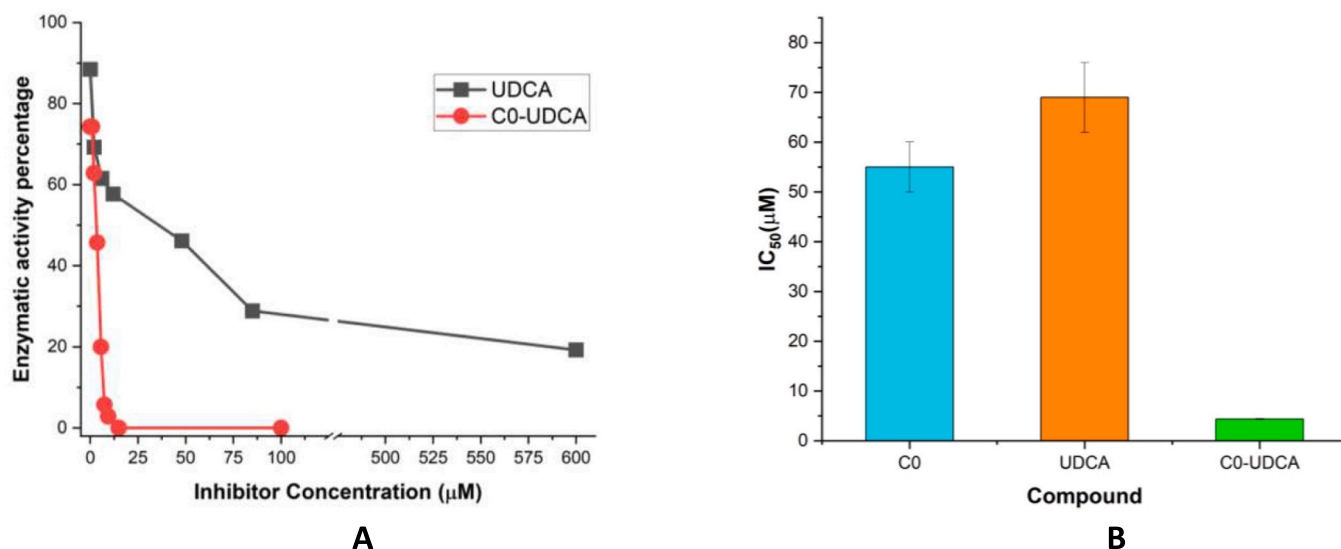
Fig. 7. Dose dependent lipoxygenase inhibition percentage of UDCA and C0-UDCA after 35 min (A). Enzymatic inhibition expressed as IC50 (concentration required to inhibit the enzymatic activity of 50%) as mean of three independent measures for C0, UDCA and C0-UDCA (B).

the IC_{50} of C0 is, for the same substrate and enzyme, $55 \pm 5 \mu M$, [18] the inhibition activity of C0-UDCA results to be 12.5 and 17 times higher than that of C0 and UDCA, respectively. These results suggest that the insertion of the UDCA auxiliary ligand in the $[Cu(phen)_2]$ core affects positively the inhibitory ability towards lipoxygenase. Moreover, the different trends shown in Fig. S10 for UDCA and C0-UDCA suggest possible different mechanisms involved in the reaction with the enzyme. A similar behaviour was observed for C0 and the mixed complex [Cu(phen)$_2$(Salubrinal)](ClO$_4$)$_2$ [18].

2.5. Soybean lipoxygenase inhibition: theoretical study

Since C0-UDCA was able to interact with Soybean Lipoxygenase, a theoretical study aiming to describe the kind of interaction was performed by Molecular Docking (MD). MD calculations were performed for UDCA-H and $[Cu(phen)_2(UDCA-H)]^+$ using the structure of Soybean Lipoxygenase (PDB:1N8Q) as receptor model. Both compounds were initially docked using a grid box centred on the Iron cofactor considering the ability of various molecules to inhibit Soybean Lipoxygenase by targeting their catalytic binding site. Results obtained for both UDCA-H and $[Cu(phen)_2(UDCA-H)]^+$ show high positive docking score values (13.42 kcal/mol and 75.96 kcal/mol respectively) that could be attributed to the hindering shape effects derived to the bulky nature of the ligands. For this reason, docking calculations on the former compounds were repeated using a grid box located between the C-terminus and N-terminus domains of Soybean Lipoxygenase. In this case, docking score values of −7.80 and − 9.39 kcal/mol were obtained for Ursodeoxycholate and $[Cu(phen)_2(UDCA-H)]^+$, respectively (Fig. S11). Analysis of the docked pose of UDCA-H (Fig. 8) indicates hydrogen bonds with Cys145 and His548 and alkyl interactions with the Val539 residue. In the case of $[Cu(phen)_2(UDCA-H)]^+$, a closer inspection of the molecular interactions (Fig. 9) reveals mainly hydrogen bond interactions with Gly265 and Gln96, carbon-hydrogen bond with Gly93 and Asn788, and π-alkyl interactions with Phe126. The conformation adopted by the highest-docking score of $[Cu(phen)_2(UDCA-H)]^+$ is stabilized by intramolecular π-sigma interactions between the ursodexoycholate moiety and one of the phenanthroline units.

These findings suggest for the studied compounds a potential allosteric inhibition mode, that might take place, for instance, by reducing the enzyme affinity for the substrate.

2.6. Cell viability study

Pancreatic cancer is considered as one of the most lethal tumors of the gastrointestinal (GI) tract, due to its difficult early diagnosis combined with its rapid progression and poor prognosis. Its incidence has been rising through the years, and it is believed that it will become the second cause of cancer-related death in the United States by 2030 [46].

On the opposite side, the incidence of ovarian cancer has been decreasing over the past decade, however, its survival rate for women in
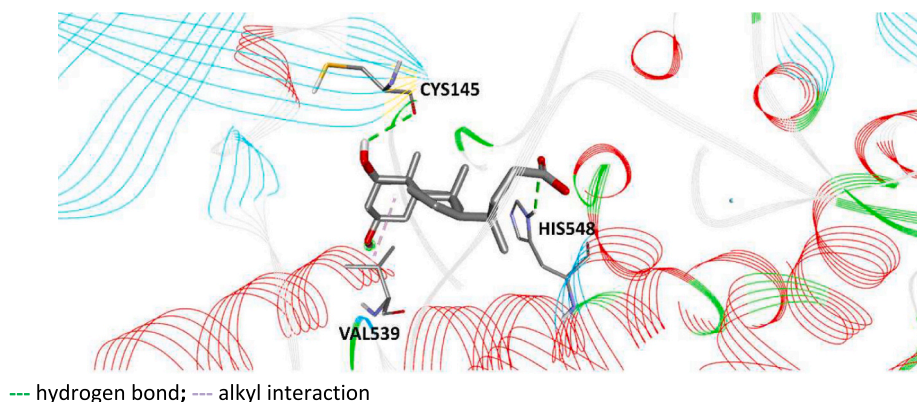

--- hydrogen bond; --- alkyl interaction

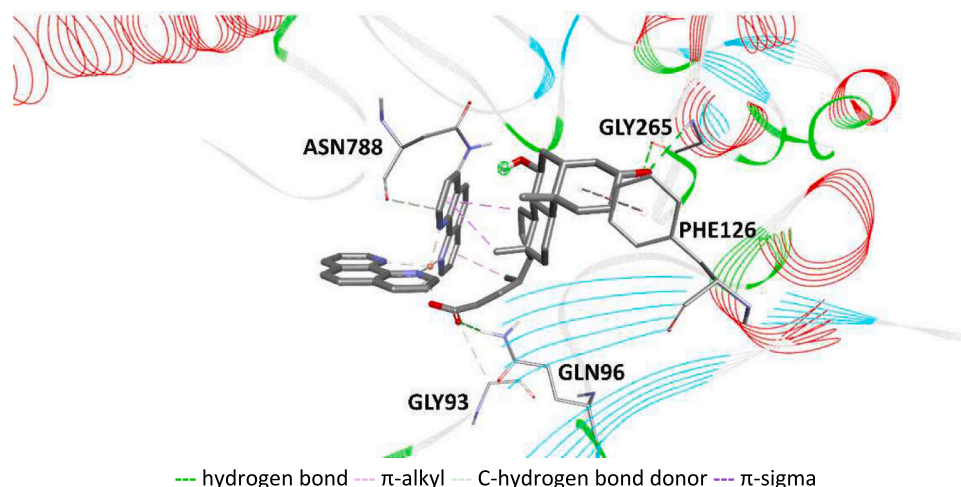**Fig. 8.** Docked pose of UDCA-H and intermolecular interactions with the surrounding residues of soybean lipoxygenase.

Fig. 9. Docked pose of $[Cu(phen)_2(UDCA-H)]^+$ and intermolecular interactions with the surrounding residues of soybean lipoxygenase.

advanced stage still remains <30%, with >80% of diagnosed patients that will experience a relapse. In addition, many patients acquire resistance towards platinum-based drugs, which are commonly used as chemotherapeutics in conjunction with surgical debulking [47].

Given these premises, we decided to evaluate the cytotoxic activity of C0-UDCA and of its precursor C0 on ovarian (SKOV-3) and pancreatic (PANC-1) cancer cells. The IC_{50} values of the studied compounds were determined from MTT results (Table 1).

In concordance to the previous reports, C0 complex reduced viability of both cell lines significantly. The C0-UDCA showed similar trend in SKOV-3 cells, and enhanced cytotoxicity in PANC-1 cell line as documented by IC_{50} values and Fig. S12. Then we determined the number of SKOV-3 and PANC-1 cancer cells treated with C0-UDCA, C0, TUDCA or left untreated, after 48 h observing a significant decrease in proliferation rate of both cell lines (Fig. 10).

To reveal, whether the reduced cell numbers are due to induction of apoptosis, we stained the intact cells with FITC-conjugated Annexin V (AV) and propidium iodide (PI). Since AV interacts with the externalized phosphatidylserine of the plasma membrane of apoptotic cells, while propidium iodide enters the cytoplasm of necrotic cells with permeable membrane, the dual staining helps to identify cell death and also to discriminate between apoptosis and necrosis Fig. 11.

Both C0-UDCA and C0 induced significant cell death as indicated by a decrease of viable cells.

In the SKOV-3 cells, C0-UDCA preferentially induced apoptosis as indicated by increase in Annexin V positive, propidium iodide negative cell (early stage apoptotic 40%, late stage apoptotic 23%, necrotic 37%) while the precursor C0 appears to act in the opposite way (necrotic 44%, early stage apoptotic 30% and late stage apoptotic 26%), as also TUDCA (necrotic 48%, early stage apoptotic 27% and late stage apoptotic 25%). In PANC-1 cells, the propidium iodide positive cells prevailed of over double positive cells, indicating secondary necrosis for both C0-UDCA (necrotic 74%, late stage apoptotic 18% and early stage apoptotic 8%) and C0 (necrotic 67%, late stage apoptotic 21% and early stage apoptotic 12%). Also TUDCA acts in same way (necrotic 58%, late stage

Table 1

Cytotoxic activity of the C0 and C0-UDCA reported as IC_{50} values (concentration of drug able to induce cell death by 50%). The standard deviation on the last significative figure is reported in parenthesis.

Compound	IC_{50} (μM)	
	SKOV-3	PANC-1
C0	7.9(1)	13.0(1)
C0-UDCA	6.8(1)	7.0(1)
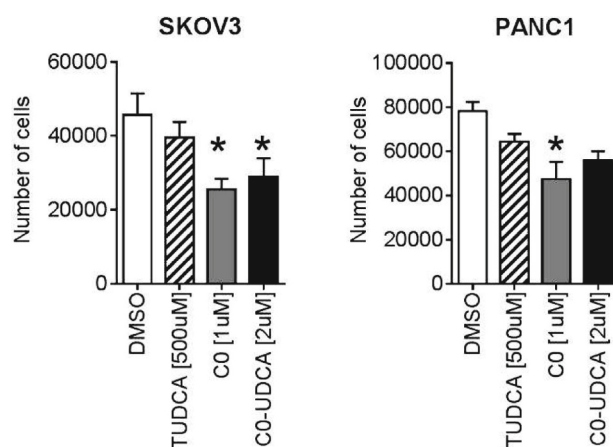
Fig. 10. The cell numbers of SKOV-3 and PANC-1 cells after 48 h culture in presence of C0, TUDCA and C0-UDCA. The starting number of cells was 20,000. Plot shows means and SDs from three independent experiments.

Fig. 11. C0-UDCA increases externalization of phosphatidylserine in SKOV-3 cells. The cells were cultured as described in the Experimental, then the exposure of phosphatidylserine on the cell surface was assessed by FACS using FITC-conjugated Annexin V probe. Cell viability was measured by propidium iodide staining. Typical results of three independent experiments are shown.

apoptotic 23% and early stage apoptotic 19%) (Fig. 11).

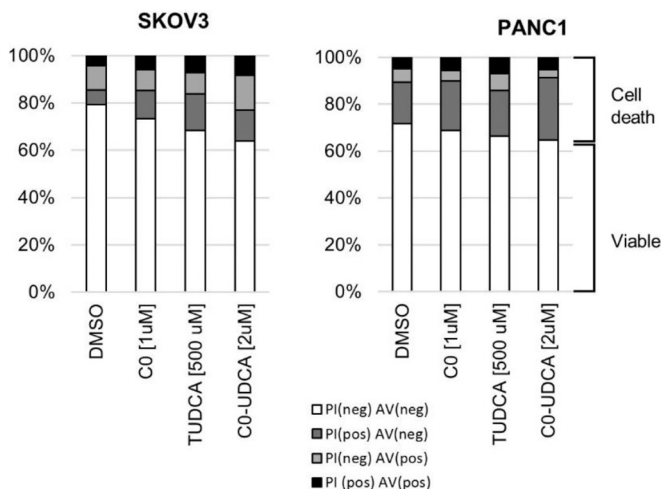### 2.7. C0-UDCA induces UPR in the cancer cell lines

As reported, UPR is major signaling pathway associated with endoplasmic reticulum responding to various sorts of cell stress [48]. To reveal the effects of C0-UDCA and its precursor C0 on UPR, we performed a western blotting (Figs. 12) and immunofluorescence staining (Fig. 13) on SKOV-3 and PANC-1 cell lines. The chemical chaperone TUDCA did not affect the levels of ER stress associated proteins in SKOV-3 cells and decreased a basal expression of CHOP protein in PANC-1 cells. On the contrary, the presence of C0 and C0-UDCA indicated the upregulation of the chaperone BiP and the pro-apoptotic protein CHOP. The activation of ER stress is also visible on the levels of the transcription factor ATF6 which levels increased especially after exposure to C0. As a control, we used 0.39 μM solution of CuSO$_4$ 5H$_2$O to exclude nonspecific, Cu-associated activation of UPR [48].

2.8. Comparison with selected structural analogues

Table 2 summarizes the anticancer activity on SKOV-3 and PANC-1 of some Cu(II) phenanthroline-based complexes along with the molecular targets investigated by the authors. In SKOV-3 cells, both C0 and C0-UDCA show potency higher than compounds a-c, comparable in the case of compounds d and m, and lower than the other complexes. As regards PANC-1 cells, both C0 and C0-UDCA are less active than the e-g complexes. A direct comparison of the mechanisms of action is not that straightforward, since many structurally similar complexes might target different pathways, while structurally different compounds might act in similar way. In addition, it is commonly known that the metal complexes might exert their biological properties by following multiple mechanisms [10], also simultaneously. In most of the cases, DNA has been reported as the primary target, since the discovery of the ability [Cu(phen)$_2$]$^+$ to act as an artificial metallonuclease by promoting the oxidative damage of DNA [49]. This result is commonly achieved by the production of ROS, as observed in the studies here cited. Interestingly, complexes (a-d) are also able to inhibit the DNA repairing process mediated by endonucleases and glycosylases, with a different extent according to N,N-diimine ligand [50]. Notably, Shi et al. have also observed how compound d is able to reduce the migration of SKOV-3 cells, inhibiting the formation of metastasis. The same compound reduces the level of Matrix Metalloprotease 2 (MMP-2), promoter or the tumour metastasis [51]. In conclusion, more efforts are still needed to have a comprehensive idea of the mechanism of action of such promising anticancer compounds.
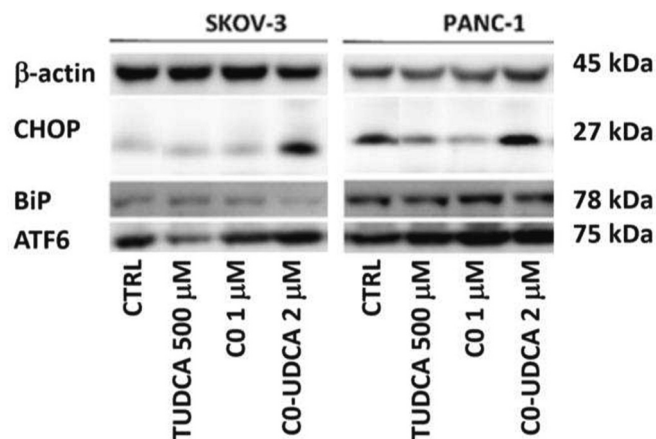
2.9. Mass spectrometry cellular fingerprints

Recently we have introduced a methodology of intact cell mass spectrometry as a tool for cell quality control, bio-typing, and cell phenotype changes identification [26,27]. Also here, we were able to detect changes in the biological background of treated cells, measuring the characteristic spectral fingerprints of individual samples. The peaks with the largest differences were selected (Fig. 14A) and a PCA statistical analysis was performed (Fig. 14B). As can be seen in Fig. 14B, it is possible to distinguish control cells from cells treated with C0, TUDCA and C0-UDCA. The clustering of specifically treated cells, indicates different effects exerted on SKOV3 cells by C0-UDCA with respect C0 or TUDCA alone.

3. Conclusions

This study shows how the chemical interaction between the [Cu(phen)$_2$(OH$_2$)]$^{2+}$ complex and the bile acid UDCA leads to the formation of the novel heteroleptic complex C0-UDCA.

Studies with lipoxygenase evidenced how the complex [Cu(phen)$_2$(UDCA-H)]$^+$ presents a anti lipoxygenase activity higher than the precursors UDCA (17×) and C0 (12.5×), showing a decrease of the concentration required to inhibit half the enzyme, from 55 μM of C0 alone or 69 of UDCA alone, to 4.4 μM of C0-UDCA. Molecular Docking studies indicate for C0-UDCA a potential allosteric mechanism. Since leukotrienes, derived from the 5-lipoxygenase pathway, are mediators of inflammation and allergy and are also involved in cardiovascular diseases, cancer and osteoporosis, the availability of molecules able to interact with 5-LOX is a challenge in the development of therapeutics, and in this field our results find an interesting scene.

Furthermore, C0-UDCA can inhibit the cell growth and reduces cell viability of both ovarian (SKOV-3) and pancreatic (PANC-1) cancer cells at micromolar level. Mechanistic studies, performed on both cell lines, indicate that this compound exerts its anticancer properties by activating the UPR pathway. In particular, in the presence of C0-UDCA the chaperone BiP and the pro-apoptotic protein CHOP are upregulated. The activation of ER stress is also visible on the levels of the transcription factor ATF6 that increased especially after exposure to C0.

The combination of IC-MALDI-MS and statistical analysis allowed us to distinguish between controls and cells treated with the C0, C0-UDCA and TUDCA compounds.

All these results, achieved thanks to the interdisciplinary approach proposed in this study, might provide new hints for the design and synthesis of novel bioactive Cu(II) coordination compounds.

4. Methods

4.1. Reagents

Acetonitrile, isopropanol, absolute ethanol, sodium linoleate, lipoxygenase, tris(hydroxymethyl)aminomethane hydrochloride (TRIS), dimethyl sulfoxide (DMSO) were purchased from Merck (Milan, Italy). Basic copper carbonate and ursodeoxycholic acid were purchased from Alfa-Aesar (Kandel, Germany). 3-(4,5-dimethylthiazol-2-yl)-2,5-diphenyltetrazolium bromide (MTT) was purchased from Sigma-Aldrich (Prague, Czech Republic). The commercial reagents were used as received, without any further purification. Ultrapure water was obtained with a MilliQ Millipore apparatus (Milan, Italy).

4.2. Mass spectrometry studies

Low resolution mass spectra were recorded using a triple quadrupole (QqQ) Varian 310-MS (Palo Alto, CA, USA) using the atmospheric-pressure ESI technique. Each sample solution was infused into the ESI source using a programmable syringe pump (1.25 mL/h constant flow rate). A dwell time of 14s was used, and the spectra were accumulated
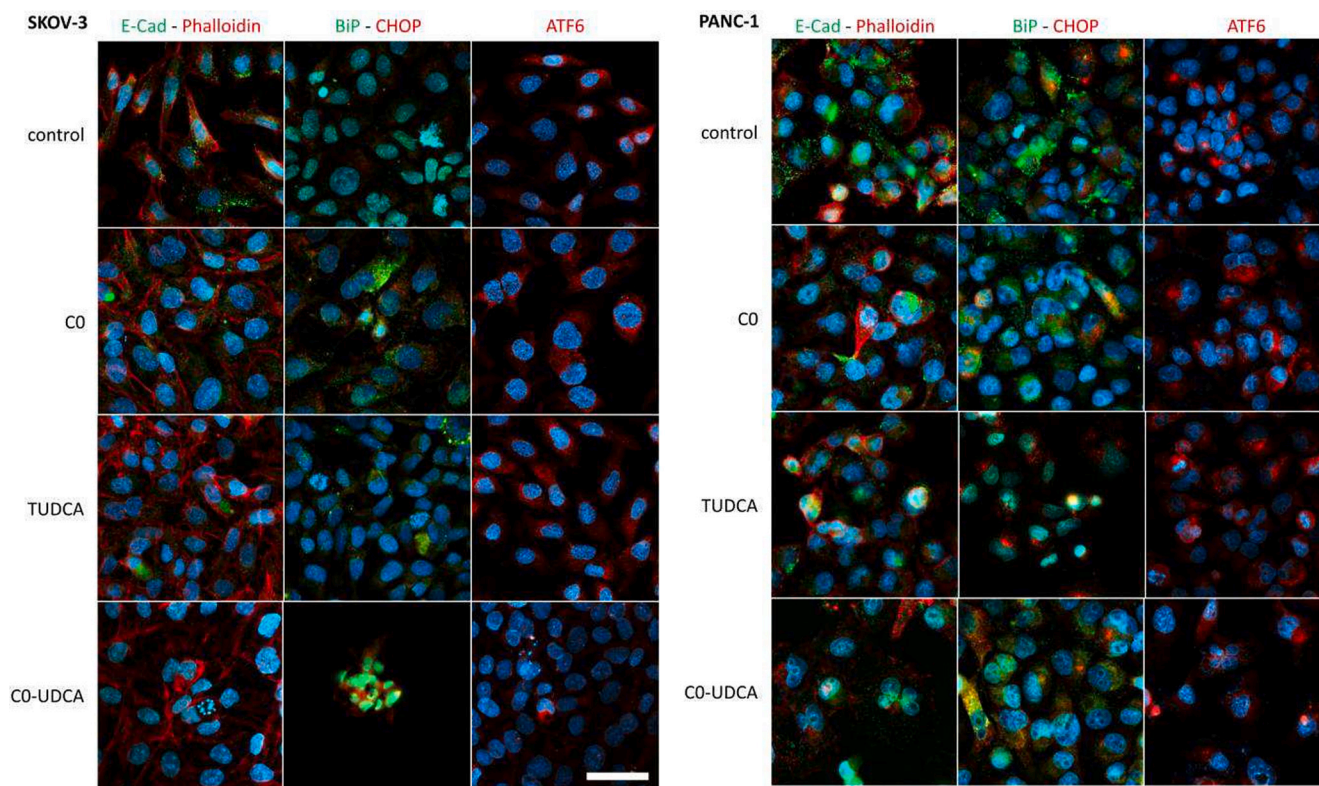

Fig. 12. Protein expression of BiP, CHOP and ATF6 in SKOV-3 and PANC-1 cells treated for 24 h with C0-UDCA at 2.0 μM. β-Actin was used as a control of equal loading.

Fig. 13. Protein levels of ER stress associated markers BiP, CHOP and ATF6. In SKOV-3 and PANC-1 cells treated for 24 h with C0, TUDCA and C0-UDCA as documented by immunofluorescence. Phalloidin was used for cytoskeleton filaments staining. Nuclei (blue) are visualized by Hoechst staining. The scale bars indicate 10 μm (for interpretation of the references to colour in this figure legend, the reader is referred to the web version of this article).

for at least 10 min to increase the signal-to-noise ratio, as previously adopted for metal complexes [54]. Mass spectra were recorded in the m/z 100–1000 range. The experimental conditions were needle voltage 3500-5000 V, shield 800 V, source temperature 60 °C, drying gas pressure 20 psi, nebulizing gas pressure 20 psi, detector voltage 1450 V. Tandem MS experiments were performed using argon as the collision gas (1.8 psi). The collision energy was varied from 5 to 50 V. High resolution mass spectra were recorded on a Thermofisher ESI-MS/MS-ORBITRAP-ELITE and Velos PRO (Waltham, MA, USA). Sample solutions were infused directly into the ESI source using a programmable syringe pump at a flow rate of 5 μL/min. Mass spectra were recorded in the m/z 600–850 range. The experimental conditions were needle voltage 2.5 kV, shield 0.8 kV, source temperature 50 °C, drying gas pressure 20 psi, nebulizing gas pressure 20 psi, detector voltage 1.3 kV. The isotopic patterns of the measured peaks in the mass spectra were analysed using the mMass 5.5.0 software package. [55,56] All the mass values are indicated as monoisotopic masses, computed as the sum of the masses of the primary isotope of each atom in the molecule (note that the monoisotopic mass may differ from the nominal molecular mass, especially for molecules having high molecular weight).

4.3. Spectroscopic studies

UV–Visible spectrophotometric measurements were performed with an Agilent Cary 60 spectrophotometer (Palo Alto, CA, USA) using a 1 cm quartz cell. UV–Vis spectra were acquired at 25 °C in the 200–1100 nm range. Solution equilibria between C0 and UDCA were evaluated by means of spectrophotometric titrations performed in phosphate buffer (0.05 M, pH 7.4). The number of linearly independent absorbing species was obtained by applying eigenvalues analysis on the absorbance data matrix. The complex formation constant, expressed as overall association constant, was calculated using the Hyperquad 2006 program. [57]

The stoichiometry of the formed complex was also evaluated using the continue variation method (Job's plot). [30,58] IR spectra were acquired with a Bruker Vector 22 spectrophotometer (Ettlingen, Germany), preparing the samples as KBr pellets.

4.4. Synthesis

4.4.1. C0

The precursor [Cu(phen)$_2$(OH$_2$)](ClO$_4$)$_2$ (C0) was prepared as previously described. [59] In brief, perchloric acid was added to an ethanolic suspension of Cu$_2$(CO$_3$)(OH)$_2$. The resulting blue solution was cooled and an ethanolic solution of 1,10-phenanthroline, at 1:2 metal: ligand molar ratio, was slowly added, observing the formation of a blue-green precipitate. This solid was filtered, washed with ethanol, and dried at room temperature (Yield 85%).
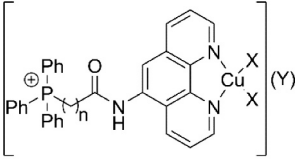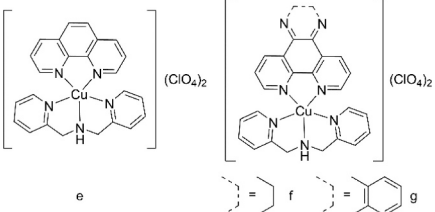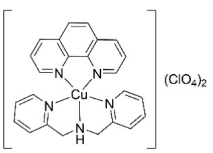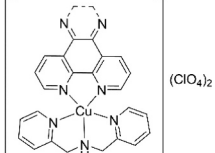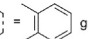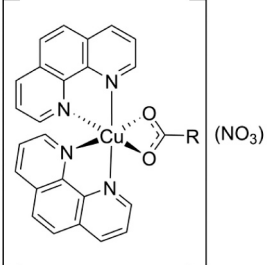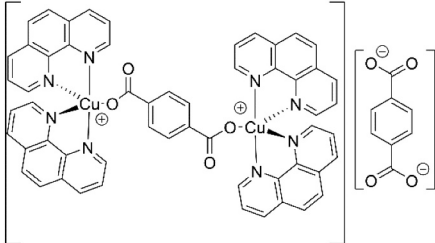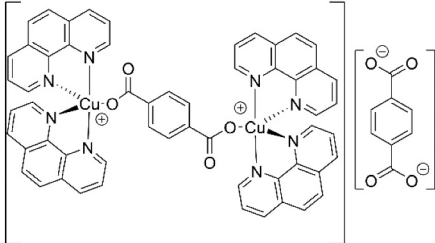
4.4.2. Sodium Ursodeoxycholate (prepared for FT-IR measurements)

UDCA (0.2318 mmol) was suspended in acetonitrile (5.0 mL), then 1 eq of NaOH 1.0 M water solution (232 μL) was added to the suspension. The reaction mixture was left under stirring at r.t. for 1 h. The product was recovered by filtration, washed with acetonitrile, and dried. 0.0411 g (Yield 43%). Elemental analysis % for C$_{24}$H$_{39}$NaO$_4$ was: expected C 69.53, H 9.48, found C 69.55, H 9.52. FT-IR (KBr), cm^{-1}: 1561 $v_{asym}(OCO)$, 1406 $v_{sym}(OCO)$.

4.4.3. C0-UDCA

[Cu(phen)$_2$(UDCA-H)](ClO$_4$) was prepared as following: UDCA (0.2385 mmol) was treated with 1 eq of NaOH to obtain the corresponding sodium salt. This solution was slowly added to a water suspension of C0 (1 eq, 10 mL). The progressive formation of a pale green precipitate was observed. The reaction mixture was stirred at room temperature for 24 h. The desired product was recovered by filtration in

Table 2
Selected Cu(II) phenanthroline-based complexes for comparison.

Compounds	IC$_{50}$ (μM)		Proposed mechanism	Ref.
	SKOV-3 cells	PANC-1 cells		
a: n = 1; X = NO$_3$, Cl; Y = NO$_3$ b: n = 4; X = Cl; Y = Br c: n = 6; X = Cl; Y = Br d: n = 8; X = Cl; Y = Br	a) 32.28 ± 2.43 b) 21.81 ± 1.57 c) 12.45 ± 1.36 d) 6.56 ± 1.28	n.a.	oxidative DNA cleavage.	[51]
	n.a.	e) 1.40 ± 0.33 f) 0.57 ± 0.19 g) 0.48 ± 0.13	ct-DNA binding.	[50]
[50] h: R = -H (CA$_1$) i: R = -CH$_3$ (CA2) j: R = -CH$_2$CH$_3$ (CA3) k: R = -CH(CH$_3$)$_2$ (CA4) l: R = -C(CH$_3$)$_3$ (CA5)	h) 2.28 ± 0.14 i) 3.04 ± 0.19 j) 3.02 ± 0.10 k) 2.86 ± 1.36 l) 3.59 ± 0.10	n.a.	ct-DNA binding.	[52]
	m) 6.7 ± 0.4	n.a.	oxidative DNA cleavage	[53]

vacuum, washed with water, diethyl ether and dried. 1.1302 g (Yield 69%). Elemental analysis % for C$_{48}$H$_{55}$ClCuN$_4$O$_8$ was: expected C 63.01, H 6.06, N 6.12, found C 63.12, H 6.11, N 6.09. ESI-MS. *m/z* found (calc.): 814.2 (814.3) for [Cu(phen)$_2$(UDCA-H)]$^+$, with the expected isotopic pattern. FT-IR (KBr), cm^{-1}: 1565, 1375 $v_{asym}(OCO)$.

4.5. Determination of the reducing activity by DPPH method

Test compounds were dissolved in DMSO at 1.0 mM concentration, then a 1:10 dilution was performed with absolute ethanol. Stock solutions of DPPH (0.1 mM, absolute ethanol) were stored in the dark and used in a few hours. 1500 μL of the test solutions were directly added in a cuvette having an equal volume of DPPH, and the absorbance (200–650 nm range) was recorded for 70 min at 25 °C. The absorbance at 517 nm was evaluated to examine the time-dependence of the radical scavenging activity. [60,61] C0, UDCA and C0UDCA did not show any reducing activity.

4.6. Soybean lipoxygenase inhibition study

Stock solutions of C0, UDCA and C0-UDCA were dissolved in DMSO at ≈ 0.1 mM concentration, then the proper dilution was performed with TRIS buffer at pH 7.4. Sodium linoleate (0.00200 g, V 10.0 mL, ≈ 0.65 mM) and soybean lipoxygenase (0.00200 g, V 10.0 mL, ≈ 2•10^{-6} M) were dissolved in TRIS buffer at pH 7.4, then the required dilutions were performed with TRIS buffer at pH 7.4. Solutions of sodium linoleate, soybean lipoxygenase and UDCA or C0-UDCA were prepared daily and kept in the dark at 5 °C. The conversion of sodium linoleate to 13-hydroperoxylinoleic acid was monitored recording the absorbance at 243 nm and compared with the appropriate standard inhibitor caffeic acid. The absorbance at 243 nm and not at 234 nm (maximum) was chosen since at 234 nm the contribution of C0 or C0-UDCA absorbance was not negligible.

4.7. DFT calculations

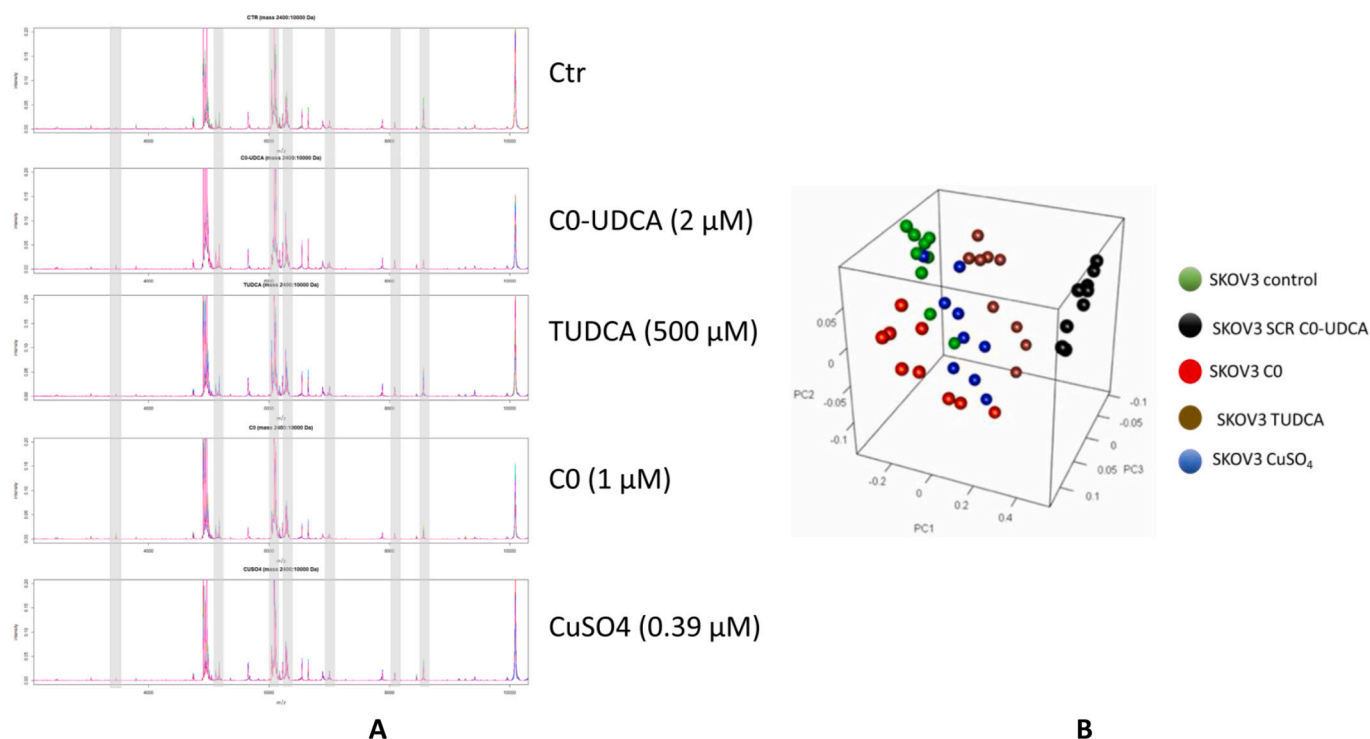Geometry optimization of deprotonated UDCA (UDCA-H) and [Cu

Fig. 14. Selected *m/z* regions of the mass spectra of treated cells, where the main differences in individual spectra are highlighted (A); PCA statistical analysis, individual treatments cluster into specific groups (B).

(phen)$_2$(UDCA-H)]$^+$ were performed on an Intel-i7 based system using the release 4.2.0 of ORCA. [62] Input files for DFT calculations were prepared using Avogadro 1.2.0. [63] Geometry optimizations were performed at DFT level, using the hybrid PBE0 functional [64] and def-2 TZVP basis set. [65] The choice of the computational setup has been made based on the results previously reported for similar Cu(II)-phenanthroline systems. [18] IR frequency calculations were carried out to verify the nature of the minima of each optimization by assessing the absence of calculated negative frequencies. Atomic charges at natural population analysis (NPA) level were calculated by means of JANPA software package. [66] Molecular orbital shapes and energies were investigated using Chemcraft v1.8. [67]

4.8. Molecular docking

Molecular docking calculations were performed using Autodock Vina software. [68] DFT-optimized structure of UDCA-H and C0-UDCA were exported as PDB files. The X-ray structure of the complex between soybean lipoxygenase and 3,4-dihydroxybenzoic acid (PDB:1N8Q) was chosen as the receptor. Prior to docking, both ligands and receptor were processed using MG Labs Autodock Tools. [69] In the receptor structure, both 3,4-dihydroxybenzoic acid (dhb) and water molecules were removed, while polar hydrogens and Gasteiger charges were added. The atomic charge for the Fe2840 cofactor was manually adjusted in the generated pdbqt file. For all the ligands, polar hydrogens and Gasteiger charges were added, while no rotational constraints were applied. Atomic charges for copper were manually adjusted in the generated pdbqt files. Validation of the docking protocol have been previously performed. [18]

The ligands were docked using a grid cube of $20 \times 20 \times 20$ points centred at Iron cofactor coordinates ($x = 21.287$, $y = 1.743$, $z = 19.171$), or using a grid cube of $30 \times 25 \times 20$ points at coordinates $x = 24.970$, $y = 11.444$, $z = -0.396$. A spacing of 1.0 Å and an exhaustiveness value of 100 was chosen in both cases. Molecular interactions and docked poses were evaluated using Biovia Discovery Studio Viewer 2021 (Dassault

Systèmes, San Diego, CA, USA).

4.9. Intact Cell MALDI-TOF MS

4.9.1. Sample preparation

Intact Cell (IC) MALDI sample preparation was described in our publications previously reported [70,71]. Briefly, matrix solution was prepared by dissolving 30 mg of Sinapinic Acid (SA) in 1 mL of CH$_3$CN/ H$_2$O/Trifluoroacetic Acid (TFA) = 70/30 obtaining 7.5% of TFA. Frozen cell pellets were thawed on ice and diluted with cold Avidin-Biotin Complex (ABC).The cell suspensions were mixed with SA matrix to reach ~25,000 cells per spot. Then, 2 μL of the resulting mixture were spotted on 384-well ground steel target on n technical replicates ($n = 5$) and dried at lab conditions.

4.9.2. Spectra acquisition

IC MALDI-TOF MS of cell populations was performed on MALDI 7090 TOF-TOF instrument equipped with 2 kHz ultra-fast solid-state UV laser (Nd-YAG: 355 nm) and variable beam focus from 10 μm to >100 μm (Shimadzu Kratos Analytical). Mass spectra were acquired in the linear positive ion mode, in mass region 2–20 kDa, pulse extraction was set to 12,5 kDa and calibration was performed externally using the Bacterial Test Standard 3.5–17 kDa (Bruker Daltonics).

5. Biological assay

5.1. Cell cultures

Ovarian cancer cell line SKOV-3 was obtained from the American Type Culture Collection (ATTC), pancreatic cell line PANC-1 was obtained as a gift from collaborating laboratory of dr. Souček. Prior to use, the cell lines were authenticated via short tandem repeat (STR) profiling, which confirmed the cell identity. Mycoplasma contamination was investigated on a routine basis using PCR. All cell lines were cultured in high glucose (4.5 g L^{-1}) Dulbecco's Modified Eagle.

Medium (DMEM) enriched with 10% fetal calf serum (FCS) (Invitrogen, Life Technologies, Czech Republic), 50 U/mL penicillin G, and 50 mg/mL streptomycin sulphate (PAA, GE Healthcare, Austria) at 37 °C in a humidified atmosphere with 5% CO_2. To specifically induce ER-stress by disruption of N-glycosylation, 1 mg/mL tunicamycin stock solution in DMSO (Sigma Aldrich, Czech Republic) was used at the indicated concentrations. ER-stress signaling was modulated by TUDCA (tauroursodeoxycholic acid, 2-[[(4R)-4-[(3R,5S,7S,8R,9S,10S,13R,14S,17R)-3,7-dihydroxy-10,13-dimethyl-2,3,4,5,6,7,8,9,11,12,14,15,16,17-tetradecahydro-1H-cyclopenta[a]phenanthren-17-yl]pentanoyl]amino]ethanesulfonic acid) dissolved in water to make 100 mg mL^{-1} stock solution (Sigma Aldrich, Czech Republic) and used at the indicated concentrations.

5.2. Cell viability assay

Cells were cultured for 24 h on a 96-well plate at a density of 10.000 cells per well in medium containing C0, TUDCA or C0-UDCA at the indicated concentrations. DMSO was used as a control. Then, the MTT reagent (3-(4,5-dimethylthiazol-2-yl)-2,5-diphenyltetrazolium bromide) (Sigma-Aldrich, Czech Republic) was added directly to the culture medium for 4 h. Then, the medium including MTT reagent was aspirated, and the cells lysed by addition of 90% isopropanol, 0.04 M HCl and 10% Triton/Tween. Absorbance was recorded at 570 nm by a Synergy HTX multi-mode reader (BioTek Instruments, VT, USA). All measurements were performed in technical pentaplicates and repeated in three independent biological experiments.

5.3. Cell growth assay

Cells were cultured for 24–72 h on a 6-well plate at a density of 20.000 cells per well in medium containing C0, TUDCA or C0-UDCA at the indicated concentrations. DMSO was used as a control. Cells were enzymatically detached, washed in Phosphate Buffer Saline (PBS) and counted using a Bürker counting chamber. Growth experiments were repeated in three independent biological experiments.

5.4. Immunofluorescence staining

Cells were cultured in 1.5H microscopic glasses, treated with compounds for 24 h and then fixed using 4% formaldehyde. Cells were washed twice with PBS and for immunofluorescent staining washed with $1\times$ PBS containing 3% BSA and 0.1% Triton X-100 and incubated with CHOP (#2895), BiP (#3177) or ATF6 (#65880) antibodies (Cell Signaling, MA, USA) of phalloidin, diluted 1:500 at room temperature for 2 h. Immunofluorescent signals were obtained by Alexa Fluor conjugated secondary antibodies (AF488, cat. no. A32731 or AF568, cat. no. A11004, both from Life Technologies, USA), diluted 1:2000. Cell nuclei were visualized by a Hoechst dye (Life Technologies, USA). Cells were then mounted and scanned by the inverted microscope Zeiss Axio Imager.

5.5. Flow cytometry

Vital staining of apoptotic cells was performed using FITC-conjugated annexin V (Roche Diagnostics, Mannheim, Germany) and propidium iodide. The cells were washed twice with staining buffer (10 mM HEPES, 140 mM NaCl, 10 mM $CaCl_2$, pH 7.4), incubated with annexin V-FITC (0.5 ll/sample) and propidium iodide (5 µg mL^{-1}) for 15 min and analysed by flow cytometry (BD FACS Aria™ II Cell Sorter). At least 10.000 viable cells were collected for each sample. Flow cytometric data were analysed using FlowJoTM 7.2.2. software (Becton–Dickinson). Results were evaluated as a percentage of double-negative cells (intact), annexin V-positive cells (early apoptotic), and double-positive (necrotic or late apoptotic) cells.

5.6. SDS-PAGE and western blotting

Trypsinised cells were washed two times with ice-cold PBS and resuspended in SDS lysis buffer (100 mM TRIS-HCl, 1% SDS, and 10% glycerol). Protein content in the cell extract was quantified using the Bradford-based BioRad protein Assay Kit (BioRad). Cell extracts were mixed with Laemmli sample buffer (100 mM Tris pH 6.8, 4% SDS, 200 mM DTT, 20% glycerol, and 0.1% bromophenol blue) and boiled for 3 min. An equivalent of 10 µg proteins was resolved using 10% sodium dodecyl sulphate polyacrylamide gel electrophoresis (SDS-PAGE). Resolved proteins were then electroblotted onto a 0.45 mm polyvinylidene difluoride (PVDF) membrane (Millipore, USA) and incubated with the indicated primary antibodies diluted 1:200–1:1000 at 4 °C overnight (Actin cat. no: Ab1801, from Abcam, UK; CHOP #2895, and BiP #3177; from Cell Signaling, MA, USA). Blots were developed using horseradish peroxidase (HRP)-conjugated anti-rabbit HRP #7074 or anti-mouse HRP #7076 (both Cell Signaling, USA) secondary antibodies, diluted 1:7500, and Immobilon Western HRP Substrate (Millipore, USA), according to the manufacturer's protocols.

CRediT authorship contribution statement

Sebastiano Masuri: Data curation, Formal analysis, Investigation, Writing – original draft. **Lukáš Moráň:** Data curation, Formal analysis, Investigation. **Tereza Vesselá:** Data curation, Investigation. **Enzo Cadoni:** Conceptualization, Formal analysis, Methodology, Project administration, Writing – original draft. **Maria Grazia Cabiddu:** Data curation, Formal analysis, Methodology, Project administration. **Lukáš Pečinka:** Data curation, Investigation. **Viktorie Gabrielová:** Data curation, Investigation. **Francesca Meloni:** Data curation, Formal analysis, Investigation. **Josef Havel:** Conceptualization, Funding acquisition, Methodology. **Petr Vaňhara:** Conceptualization, Formal analysis, Funding acquisition, Methodology, Resources, Writing – original draft, Supervision, Validation, Visualization. **Tiziana Pivetta:** Conceptualization, Formal analysis, Funding acquisition, Methodology, Project administration, Resources, Writing – original draft, Supervision, Validation, Visualization.

Declaration of Competing Interest

Data availability

Data will be made available on request.

Acknowledgments

Appendix A. Supplementary data

Supplementary data to this article can be found online at https://doi.

org/10.1016/j.jinorgbio.2023.112301.

References

[1] J.-F. Goossens, C. Bailly, Ursodeoxycholic acid and cancer: from chemoprevention to chemotherapy, Pharmacol. Ther. 203 (2019), 107396, https://doi.org/10.1016/j.pharmthera.2019.107396.

[2] L. Dyakova, D.C. Culita, G. Marinescu, M. Alexandrov, R. Kalfin, L. Patron, R. Alexandrova, Metal Zn(II), Cu(II), Ni (II) complexes of ursodeoxycholic acid as putative anticancer agents, Biotechnol. Biotechnol. Equip. 28 (2014) 543–551, https://doi.org/10.1080/13102818.2014.927973.

[3] J. Chung, S.H. An, S.W. Kang, K. Kwon, Ursodeoxycholic acid (UDCA) exerts anti-atherogenic effects by inhibiting RAGE signaling in diabetic atherosclerosis, PLoS One 11 (2016) 1–18, https://doi.org/10.1371/journal.pone.0147839.

[4] U. Beuers, J.L. Boyer, G. Paumgartner, Ursodeoxycholic acid in cholestasis: potential mechanisms of action and therapeutic applications, Hepatology 28 (1998) 1449–1453, https://doi.org/10.1002/hep.510280601.

[5] J.-F. Goossens, C. Bailly, Ursodeoxycholic acid and cancer: from chemoprevention to chemotherapy, Pharmacol. Ther. 203 (2019), 107396, https://doi.org/10.1016/j.pharmthera.2019.107396.

[6] A.L. Cao, L. Wang, X. Chen, Y.M. Wang, H.J. Guo, S. Chu, C. Liu, X.M. Zhang, W. Peng, Ursodeoxycholic acid and 4-phenylbutyrate prevent endoplasmic reticulum stress-induced podocyte apoptosis in diabetic nephropathy, Lab. Investig. 96 (2016) 610–622, https://doi.org/10.1038/labinvest.2016.44.

[7] E.J. Anthony, E.M. Bolitho, H.E. Bridgewater, O.W.L. Carter, J.M. Donnelly, C. Imberti, E.C. Lant, F. Lermyte, R.J. Needham, M. Palau, P.J. Sadler, H. Shi, F.-X. Wang, W.-Y. Zhang, Z. Zhang, Metallodrugs are unique: opportunities and challenges of discovery and development, Chem. Sci. 11 (2020) 12888–12917, https://doi.org/10.1039/D0SC04082G.

[8] F. Trudu, F. Amato, P. Vaňhara, T. Pivetta, E.M. Peña-Méndez, J. Havel, Coordination compounds in cancer: past, present and perspectives, J. Appl. Biomed. 13 (2015) 79–103, https://doi.org/10.1016/j.jab.2015.03.003.

[9] C. Santini, M. Pellei, V. Gandin, M. Porchia, F. Tisato, C. Marzano, Advances in copper complexes as anticancer agents, Chem. Rev. 114 (2014) 815–862, https://doi.org/10.1021/cr400135x.

[10] S. Masuri, P. Vaňhara, M.G. Cabiddu, L. Morán, J. Havel, E. Cadoni, T. Pivetta, Copper(II) phenanthroline-based complexes as potential anticancer drugs: a walkthrough on the mechanisms of action, Molecules 27 (2022) 49, https://doi.org/10.3390/molecules27010049.

[11] D. Denoyer, S. Masaldan, S. La Fontaine, M.A. Cater, Targeting copper in cancer therapy: 'copper that cancer', Metallomics 7 (2015) 1459–1476, https://doi.org/10.1039/c5mt00149h.

[12] E.J, L.I.E. Balsa, M. Lucia, Baran, Copper complexes as antitumor agents: in vitro and in vivo evidence, Curr. Med. Chem. 30 (2023) 510–557.

[13] R. Galindo-Murillo, J.C. García-Ramos, L. Ruiz-Azuara, T.E. Cheatham III, F. Cortés-Guzmán, Intercalation processes of copper complexes in DNA, Nucleic Acids Res. 43 (2015) 5364–5376, https://doi.org/10.1093/nar/gkv467.

[14] Z. Zhang, H. Wang, M. Yan, H. Wang, C. Zhang, Novel copper complexes as potential proteasome inhibitors for cancer treatment (review), Mol. Med. Rep. 15 (2017) 3–11, https://doi.org/10.3892/mmr.2016.6022.

[15] L.M. Balsa, V. Ferraresi-Curotto, M.J. Lavecchia, G.A. Echeverría, O.E. Piro, J. García-Tojal, R. Pis-Diez, A.C. González-Baró, I.E. León, Anticancer activity of a new copper(ii) complex with a hydrazone ligand. Structural and spectroscopic characterization, computational simulations and cell mechanistic studies on 2D and 3D breast cancer cell models, Dalton Trans. 50 (2021) 9812–9826, https://doi.org/10.1039/d1dt00869b.

[16] P. Levín, M.C. Ruiz, A.I.B. Romo, O.R. Nascimento, A.L. Di Virgilio, A.G. Oliver, A. P. Ayala, I.C.N. Diógenes, I.E. León, L. Lemus, Water-mediated reduction of [Cu (dmp)$_2$(CH$_3$CN)]$^{2+}$: implications of the structure of a classical complex on its activity as an anticancer drug, Inorg. Chem. Front. 8 (2021) 3238–3252, https://doi.org/10.1039/D1QI00233C.

[17] L. Morán, T. Pivetta, S. Masuri, K. Vašíčková, F. Walter, J. Prehn, M. Elkalaf, J. Trnka, J. Havel, P. Vaňhara, Mixed copper(II)–phenanthroline complexes induce cell death of ovarian cancer cells by evoking the unfolded protein response, Metallomics 11 (2019) 1481–1489, https://doi.org/10.1039/C9MT00055K.

[18] S. Masuri, E. Cadoni, M.G. Cabiddu, F. Isaia, M.G. Demuru, L. Morán, D. Buček, P. Vaňhara, J. Havel, T. Pivetta, The first copper(II) complex with 1,10-phenanthroline and salubrinal with interesting biochemical properties, Metallomics 12 (2020) 891–901, https://doi.org/10.1039/D0MT00006J.

[19] R. Sano, J.C. Reed, ER stress-induced cell death mechanisms, Biochim. Biophys. Acta, Mol. Cell Res. 2013 (1833) 3460–3470, https://doi.org/10.1016/j.bbamcr.2013.06.028.

[20] V. Gandin, M. Pellei, F. Tisato, M. Porchia, C. Santini, C. Marzano, A novel copper complex induces paraptosis in colon cancer cellsviathe activation of ER stress signalling, J. Cell. Mol. Med. 16 (2012) 142–151, https://doi.org/10.1111/j.1582-4934.2011.01292.x.

[21] R. Bortolozzi, G. Viola, E. Porcù, F. Consolaro, C. Marzano, M. Pellei, V. Gandin, G. Basso, A novel copper(I) complex induces ER-stress-mediated apoptosis and sensitizes B-acute lymphoblastic leukemia cells to chemotherapeutic agents, Oncotarget 5 (2014) 5978–5991, https://doi.org/10.18632/oncotarget.2027.

[22] S. Tardito, C. Isella, E. Medico, L. Marchiò, E. Bevilacqua, M. Hatzoglou, O. Bussolati, R. Franchi-Gazzola, The thioxotriazole copper (II) complex A0 induces endoplasmic reticulum stress and paraptotic death in human cancer cells, J. Biol. Chem. 284 (2009) 24306–24319, https://doi.org/10.1074/jbc.M109.026583.

[23] L.M. Balsa, M.R. Rodriguez, V. Ferraresi-Curotto, B.S. Parajón-Costa, A. C. Gonzalez-Baró, I.E. León, Finding new molecular targets of two copper(II)-hydrazone complexes on triple-negative breast cancer cells using mass-spectrometry-based quantitative proteomics, Int. J. Mol. Sci. 24 (2023), https://doi.org/10.3390/ijms24087531.

[24] S. Munshi, R. Dahl, Cytoprotective small molecule modulators of endoplasmic reticulum stress, Bioorg. Med. Chem. 24 (2016) 2382–2388, https://doi.org/10.1016/j.bmc.2016.03.045.

[25] U. Ozcan, E. Yilma, L. Özcan, E. Furuhashi, E. Vaillancourt, R.O. Smith, C. Z. Görgün, G.S. Hotamisligil, Chemical chaperones reduce ER stress and restore glucose homeostasis in a mouse model of type 2 diabetes, Science 313 (2006) (1979) 1137–1140, https://doi.org/10.1126/science.1128294.

[26] P. Vaňhara, L. Morán, L. Pečinka, V. Porokh, T. Pivetta, S. Masuri, E. Maria Peña-Méndez, J. Elías Conde González, A. Hampl, J. Havel, Intact cell mass spectrometry for embryonic stem cell biotyping, in: Mass Spectrometry in Life Sciences and Clinical Laboratory, IntechOpen, 2021, https://doi.org/10.5772/intechopen.95074.

[27] P. Vaňhara, L. Kučera, L. Prokeš, L. Jurečková, E.M. Peña-Méndez, J. Havel, A. Hampl, Intact cell mass spectrometry as a quality control tool for revealing minute phenotypic changes of cultured human embryonic stem cells, Stem Cells Transl. Med. 7 (2018) 109–114, https://doi.org/10.1002/sctm.17-0107.

[28] C. Hao, R.E. March, Electrospray ionization tandem mass spectrometric study of salt cluster ions: part 2 : salts of polyatomic acid groups and of multivalent metals, J. Mass Spectrom. 36 (2001) 509–521, https://doi.org/10.1002/jms.150.

[29] P. Job, Formation and Stability of Inorganic Complexes in Solution, Ann. Chim. Appl. 9 (1928) 113–203.

[30] J.S. Renny, L.L. Tomasevich, E.H. Tallmadge, D.B. Collum, Method of continuous variations: applications of job plots to the study of molecular associations in organometallic chemistry, Angew. Chem. Int. Ed. 52 (2013) 11998–12013, https://doi.org/10.1002/anie.201304157.

[31] G. Deacon, R.J. Phillips, Relationships between the carbon-oxygen stretching frequencies of carboxylato complexes and the type of carboxylate coordination, Coord. Chem. Rev. 33 (1980) 227–250, https://doi.org/10.1016/S0010-8545(00)80455-5.

[32] K. Nakamoto, Infrared and Raman Spectra of Inorganic and Coordination Compounds, John Wiley & Sons, Inc., Hoboken, NJ, USA, 2008, https://doi.org/10.1002/9780470405840.

[33] A.W. Addison, T.N. Rao, J. Reedijk, J. van Rijn, G.C. Verschoor, Synthesis, structure, and spectroscopic properties of copper(II) compounds containing nitrogen–sulphur donor ligands; the crystal and molecular structure of aqua[1,7-bis(N-methylbenzimidazol-2′-yl)-2,6-dithiaheptane]copper(II) pe, J. Chem. Soc. Dalton Trans. (1984) 1349–1356, https://doi.org/10.1039/DT9840001349.

[34] M. Devereux, M. McCann, J.F. Cronin, G. Ferguson, V. McKee, Binuclear and polymeric copper(II) dicarboxylate complexes: syntheses and crystal structures of [Cu$_2$(pda)(Phen)$_4$](ClO$_4$)$_2$·5H$_2$O·C$_2$H$_5$OH, [Cu$_2$(oda)(Phen)$_4$] (ClO$_4$)$_2$·2.67H$_2$O·C$_2$H$_5$OH and {[Cu$_2$(pda)$_2$(NH$_3$)$_4$(H$_2$O)$_2$]·4H$_2$O}n (odaH$_2$=octanedioic acid; pdaH$_2$=pentanedioic a), Polyhedron 18 (1999) 2141–2148, https://doi.org/10.1016/S0277-5387(99)00100-X.

[35] F. Clifford, E. Counihan, W. Fitzgerald, K. Seff, C. Simmons, S. Tyagi, B. Hathaway, The crystal structures of [Cu(phen)$_2$(O$_2$CMe)]X (phen = 1,10-phenanthroline) complexes: pseudo cis-distorted octahedral structures and fluxional copper(II) stereochemistries, J. Chem. Soc. Chem. Commun. (1982) 196, https://doi.org/10.1039/c39820000196.

[36] M. Barceló-Oliver, Á. García-Raso, Á. Terrón, E. Molins, M.J. Prieto, V. Moreno, J. Martínez, V. Lladó, I. López, A. Gutiérrez, P.V. Escribá, Synthesis and mass spectroscopy kinetics of a novel ternary copper(II) complex with cytotoxic activity against cancer cells, J. Inorg. Biochem. 101 (2007) 649–659, https://doi.org/10.1016/j.jinorgbio.2006.12.008.

[37] K.N. Lazarou, S.P. Perlepes, V. Psycharis, C.P. Raptopoulou, Synthetic study of the ternary copper(II)/maleamate(−1)/1,10-phenanthroline reaction system: mononuclear, dinuclear and polymeric complexes, Polyhedron 27 (2008) 2131–2142, https://doi.org/10.1016/j.poly.2008.04.005.

[38] A.R. Brash, Lipoxygenases: occurrence, functions, catalysis, and acquisition of substrate, J. Biol. Chem. 274 (1999) 23679–23682, https://doi.org/10.1074/jbc.274.34.23679.

[39] Erik W. Thompson, Donald F. Newgreen, Carcinoma invasion and metastasis: a role for epithelial-mesenchymal transition? Cancer Res. 65 (2005) 5991–5995.

[40] R. Yoshimura, M. Matsuyama, K. Tsuchida, Y. Kawahito, H. Sano, T. Nakatani, Expression of lipoxygenase in human bladder carcinoma and growth inhibition by its inhibitors, J. Urol. 170 (2003) 1994–1999, https://doi.org/10.1097/01.ju.0000080296.54262.c8.

[41] X. Chen, S. Wang, N. Wu, S. Sood, P. Wang, Z. Jin, D.G. Beer, T.J. Giordano, Y. Lin, W.-C.J. Shih, R.A. Lubet, C.S. Yang, Overexpression of 5-Lipoxygenase in Rat and Human Esophageal Adenocarcinoma and Inhibitory Effects of Zileuton and Celecoxib on Carcinogenesis, Clin. Cancer. Res (2004). 6703-6709 http://aacrjournals.org/clincancerres/article-pdf/10/19/6703/1954466/zdf01904006703.pdf.

[42] X.M. Xu, J.J. Deng, G.J. Yuan, F. Yang, H.T. Guo, M. Xiang, W. Ge, Y.G. Wu, 5-lipoxygenase contributes to the progression of hepatocellular carcinoma, Mol. Med. Rep. 4 (2011) 1195–1200, https://doi.org/10.3892/mmr.2011.547.

[43] M.P. Wasilewicz, B. Kołodziej, T. Bojułko, M. Kaczmarczyk, V. Sulżyc-Bielicka, D. Bielicki, K. Ciepiela, Overexpression of 5-lipoxygenase in sporadic colonic adenomas and a possible new aspect of colon carcinogenesis, Int. J. Color. Dis. 25 (2010) 1079–1085, https://doi.org/10.1007/s00384-010-0980-z.

[44] Masahide Matsuyama, Rikio Yoshimura, Makoto Mitsuhashi, Taro Hase, Kenji Tsuchida, Yoshiaki Takemoto, Yutaka Kawahito, Hajime Sano,

Tatsuya Nakatani, Expression of lipoxygenase in human prostate cancer and growth reduction by its inhibitors, Int. J. Oncol. (2004) 821–827.

[45] R. Wisastra, F. Dekker, Inflammation, cancer and oxidative lipoxygenase activity are intimately linked, Cancers (Basel) 6 (2014) 1500–1521, https://doi.org/10.3390/cancers6031500.

[46] L. Rahib, B.D. Smith, R. Aizenberg, A.B. Rosenzweig, J.M. Fleshman, L. M. Matrisian, Projecting cancer incidence and deaths to 2030: the unexpected burden of thyroid, liver, and pancreas cancers in the United States, Cancer Res. 74 (2014) 2913–2921, https://doi.org/10.1158/0008-5472.can-14-0155.

[47] B.R. Corr, M. Moroney, J. Sheeder, S.G. Eckhardt, B. Sawyer, K. Behbakht, J. R. Diamond, Survival and clinical outcomes of patients with ovarian cancer who were treated on phase 1 clinical trials, Cancer 126 (2020) 4289–4293, https://doi.org/10.1002/cncr.33073.

[48] K. Kratochvílová, L. Moráň, S. Paďourová, S. Stejskal, L. Tesařová, P. Šimara, A. Hampl, I. Koutná, P. Vaňhara, The role of the endoplasmic reticulum stress in stemness, pluripotency and development, Eur. J. Cell Biol. 95 (2016) 115–123, https://doi.org/10.1016/j.ejcb.2016.02.002.

[49] D.S. Sigman, D.R. Graham, V.D. Aurora, A.M. Stern, Oxygen-dependent cleavage of DNA by the 1,10-phenanthroline cuprous complex, J. Biol. Chem. 254 (1979) 12269–12272.

[50] N.Z. Fantoni, Z. Molphy, S. O'Carroll, G. Menounou, G. Mitrikas, M.G. Krokidis, C. Chatgilialoglu, J. Colleran, A. Banasiak, M. Clynes, S. Roche, S. Kelly, V. McKee, A. Kellett, Polypyridyl-based copper phenanthrene complexes: combining stability with enhanced DNA recognition, Chem. Eur. J. 27 (2021) 971–983, https://doi.org/10.1002/chem.202001996.

[51] X. Shi, Z. Chen, Y. Wang, Z. Guo, X. Wang, Hypotoxic copper complexes with potent anti-metastatic and anti-angiogenic activities against cancer cells, Dalton Trans. 47 (2018) 5049–5054, https://doi.org/10.1039/c8dt00794b.

[52] A. Prisecaru, V. McKee, O. Howe, G. Rochford, M. McCann, J. Colleran, M. Pour, N. Barron, N. Gathergood, A. Kellett, Regulating bioactivity of Cu2+ Bis-1,10-phenanthroline artificial metallonucleases with sterically functionalized pendant carboxylates, J. Med. Chem. 56 (2013) 8599–8615, https://doi.org/10.1021/jm401465m.

[53] A. Prisecaru, M. Devereux, N. Barron, M. McCann, J. Colleran, A. Casey, V. McKee, A. Kellett, Potent oxidative DNA cleavage by the di-copper cytotoxin: [Cu2 (μ-terephthalate)(1,10-phen)4]2+n, Chem. Commun. 48 (2012) 6906–6908, https://doi.org/10.1039/c2cc31023f.

[54] F. Isaia, M.C. Aragoni, M. Arca, C. Caltagirone, C. Castellano, G. de Filippo, A. Garau, V. Lippolis, T. Pivetta, Gold and palladium oxidation/complexation in water by a thioamide-iodine leaching system, Green Chem. 19 (2017) 4591–4599, https://doi.org/10.1039/c7gc01310h.

[55] M. Strohalm, D. Kavan, P. Nova, M. Volny, mMass 3 : a cross-platform software environment for precise analysis of mass spectrometric data, Anal. Chem. 82 (2010) 4648–4651.

[56] T.H.J. Niedermeyer, M. Strohalm, mMass as a software tool for the annotation of cyclic peptide tandem mass spectra, PLoS One 7 (2012), e44913, https://doi.org/10.1371/journal.pone.0044913.

[57] P. Gans, A. Sabatini, A. Vacca, Investigation of equilibria in solution. Determination of equilibrium constants with the HYPERQUAD suite of programs, Talanta 43 (1996) 1739–1753, https://doi.org/10.1016/0039-9140(96)01958-3.

[58] P. Caumul, K. Boodhoo, S.B. Burkutally, S. Seeruttun, N. Namooya, N. Ramsahye, Synthesis and Analysis of Metal Chelating Amino and Diamine Precursors andtheir Complex Formation on Copper (II) using Conductivity and SpectroscopicMethods, Res. J. Pharm. Biol. Chem. Sci. 10 (2) (2014) 494–509.

[59] T. Pivetta, M.D. Cannas, F. Demartin, C. Castellano, S. Vascellari, G. Verani, F. Isaia, Synthesis, structural characterization, formation constants and in vitro cytotoxicity of phenanthroline and imidazolidine-2-thione copper(II) complexes, J. Inorg. Biochem. 105 (2011) 329–338, https://doi.org/10.1016/j.jinorgbio.2010.11.017.

[60] C. Tolia, A.N. Papadopoulos, C.P. Raptopoulou, V. Psycharis, C. Garino, L. Salassa, G. Psomas, Copper (II) interacting with the non-steroidal antiinflammatory drug flufenamic acid : structure, antioxidant activity and binding to DNA and albumins, J. Inorg. Biochem. 123 (2013) 53–65, https://doi.org/10.1016/j.jinorgbio.2013.02.009.

[61] Z. Boulsourani, G.D. Geromichalos, S. Katsamakas, V. Psycharis, C.P. Raptopoulou, Materials science & engineering C mononuclear copper (II) complexes with 2-thiophene carboxylate and N-N donors ; DNA interaction, antioxidant / anti-inflammatory and antitumor activity, Mater. Sci. Eng. C 94 (2019) 493–508, https://doi.org/10.1016/j.msec.2018.09.059.

[62] F. Neese, The ORCA program system, Wiley Interdiscip. Rev. Comput. Mol. Sci. 2 (2012) 73–78, https://doi.org/10.1002/wcms.81.

[63] M.D. Hanwell, D.E. Curtis, D.C. Lonie, T. Vandermeersch, E. Zurek, G.R. Hutchison, Avogadro: an advanced semantic chemical editor, visualization, and analysis platform, Aust. J. Chem. 4 (2012) 17, https://doi.org/10.1186/1758-2946-4-17.

[64] C. Adamo, V. Barone, Toward reliable density functional methods without adjustable parameters: the PBE0 model, J. Chem. Phys. 110 (1999) 6158–6170, https://doi.org/10.1063/1.478522.

[65] F. Weigend, R. Ahlrichs, Balanced basis sets of split valence, triple zeta valence and quadruple zeta valence quality for H to Rn: design and assessment of accuracy, Phys. Chem. Chem. Phys. 7 (2005) 3297–3305, https://doi.org/10.1039/b508541a.

[66] T.Y. Nikolaienko, L.A. Bulavin, D.M. Hovorun, JANPA: an open source cross-platform implementation of the natural population analysis on the Java platform, Comput. Theor. Chem. 1050 (2014) 15–22, https://doi.org/10.1016/j.comptc.2014.10.002.

[67] Chemcraft, Graphical Software for Visualization of Quantum Chemistry Computations. https://www.chemcraftprog.com.

[68] O. Trott, A.J. Olson, AutoDock Vina: improving the speed and accuracy of docking with a new scoring function, efficient optimization, and multithreading, J. Comput. Chem. (2009) 455–461, https://doi.org/10.1002/jcc.21334.

[69] G.M. Morris, H. Ruth, W. Lindstrom, M.F. Sanner, R.K. Belew, D.S. Goodsell, A. J. Olson, Software news and updates AutoDock4 and AutoDockTools4: automated docking with selective receptor flexibility, J. Comput. Chem. 30 (2009) 2785–2791, https://doi.org/10.1002/jcc.21256.

[70] M. Deulofeu, L. Kolářová, V. Salvadó, E. María Peña-Méndez, M. Almáši, M. Štork, L. Pour, P. Boadas-Vaello, S. Ševčíková, J. Havel, J. Havel, P. Vaňhara, Rapid discrimination of multiple myeloma patients by artificial neural networks coupled with mass spectrometry of peripheral blood plasma, Sci. Rep. 9 (2019), https://doi.org/10.1038/s41598-019-44215-1.

[71] E. Valletta, L. Kučera, L. Prokeš, F. Amato, T. Pivetta, A. Hampl, J. Havel, P. Vaňhara, Multivariate calibration approach for quantitative determination of cell-line cross contamination by intact cell mass spectrometry and artificial neural networks, PLoS One 11 (2016), https://doi.org/10.1371/journal.pone.0147414.